Holocene evolution in weathering and erosion patterns in the Pearl River delta

Dengke Hu

School of Geosciences, University of Aberdeen, Aberdeen, AB24 3UE, UK (dhu@abdn.ac.uk)

Key Laboratory of Marginal Sea Geology, Chinese Academy of Sciences, Guangzhou, China

Peter D. Clift

Department of Geology and Geophysics, Louisiana State University, Baton Rouge, Louisiana, USA

Key Laboratory of Marginal Sea Geology, Chinese Academy of Sciences, Guangzhou, China

Philipp Böning

Institute of Chemistry and Biology of the Marine Environment (ICBM), Carl von Ossietzky University of Oldenburg, Oldenburg, Germany

Robyn Hannigan

Department of Environmental, Earth and Ocean Sciences, University of Massachusetts-Boston, Boston, Massachusetts, USA

Stephen Hillier

Group of Environmental and Biochemical Sciences, The James Hutton Institute, Craigiebuckler, Aberdeen, UK

Department of Soil and Environment, Swedish University of Agricultural Sciences, Sweden

Jerzy Blusztajn

Department of Geology and Geophysics, Woods Hole Oceanographic Institution, Woods Hole, Massachusetts, USA

Shiming Wan

Key Laboratory of Marine Geology and Environment, Institute of Oceanology, Chinese Academy of Sciences, Qingdao, China

Dorian Q. Fuller

Institute of Archaeology, University College London, London, UK

[1] Sediments in the Pearl River delta have the potential to record the weathering response of this river basin to climate change since 9.5 ka, most notably weakening of the Asian monsoon since the Early Holocene (∼8 ka). Cores from the Pearl River delta show a clear temporal evolution of weathering intensity, as measured by K/Al, K/Rb, and clay mineralogy, that shows deposition of less weathered sediment at a time of weakening monsoon rainfall in the Early-Mid Holocene (6.0–2.5 ka). This may reflect an immediate response to a less humid climate, or more likely reduced reworking of older deposits from river terraces as the monsoon weakened. Human settlement of the Pearl River basin may have had a major impact on landscape and erosion as a result of the establishment of widespread agriculture. After around 2.5 ka weathering intensity sharply increased, despite limited change in the monsoon, but at a time when anthropogenic pollutants (e.g., Cu, Zn, and Pb) increased and when the flora of the basin

changed. $^{87}Sr/^{86}Sr$ covaries with these other proxies but is also partly influenced by the presence of carbonate. The sediments in the modern Pearl River are even more weathered than the youngest material from the delta cores. We infer that the spread of farming into the Pearl River basin around 2.7 ka was followed by a widespread reworking of old, weathered soils after 2.5 ka, and large-scale disruption of the river system that was advanced by 2.0 ka.

1. Introduction

[2] Delta sediments can be used to reconstruct the history of erosion and weathering in the drainage basin from which the river derives its load and is expected to reflect landscape in the basin at the time of deposition. Erosion and weathering rates are known to be closely linked with climatic processes because warmer and wetter conditions generally favor faster erosion and more intensive chemical weathering [*Edmond and Huh*, 1997; *West et al.*, 2005; *White and Blum*, 1995]. Sediment chemistry reflects the composition of the original bedrock source, the intensity of chemical weathering, the degree of reworking in the river basin, and the influence of sediment transport in the river. The effects of tidal and long-shore current activity can also be significant because muddy and sandy sediments have different composition even when derived from the same sources in the same environment [*Garrels and MacKenzie*, 1971; *Shao et al.*, 2012].

[3] Despite these complexities, marine sediments can and have been used to reconstruct environmental conditions in the source regions, although this is dependent on provenance being constrained [*Colin et al.*, 2010; *Derry and France-Lanord*, 1996; *Wan et al.*, 2009]. In SE Asia the climate is dominated by the Asian monsoon system, which has varied since the last glacial maximum [*Dykoski et al.*, 2005; *Wang et al.*, 2001] provid-

ing the chance to see how landscape has responded to this forcing. We have examined the sedimentary record of the Pearl River since 9.5 ka in order to see how the weathering state and provenance of sediment in the delta has changed since that time, in order to understand how the river basin environment responded to climatic changes.

2. Geological and Climatic Setting

[4] The Pearl River extends around 2400 km and drains 409,000 km² of southern China, a hilly but not very tectonically active region (Figure 1a). Elevations extend from close to sea level and run up to around 2100 m in the upper reaches. Locally gradients can be steep and there are peaks >1900 m in the central part of the basin. The river drains a wide variety of rock types, with the eastern and southern parts of the basin dominated by granites and minor amounts of volcanic rock [*Jahn et al.*, 1990]. In addition, there are Jurassic and Cretaceous rift basins overlying the basement. Toward the NW the basin contains wide expanse of Late Palaeozoic carbonate rocks [*Chen et al.*, 2001], Triassic dolomites and siliciclastic continental red-bed rocks. The river itself postdates the rifting of the South China Sea, starting in the Eocene [*Clift et al.*, 2001; *Ru and Pigott*, 1986]. At present most of the Pearl River basin experiences a humid subtropical climate, with conditions reaching almost tropical levels in the far south. Near the delta winter temperatures average 18°C, rising to 33°C in
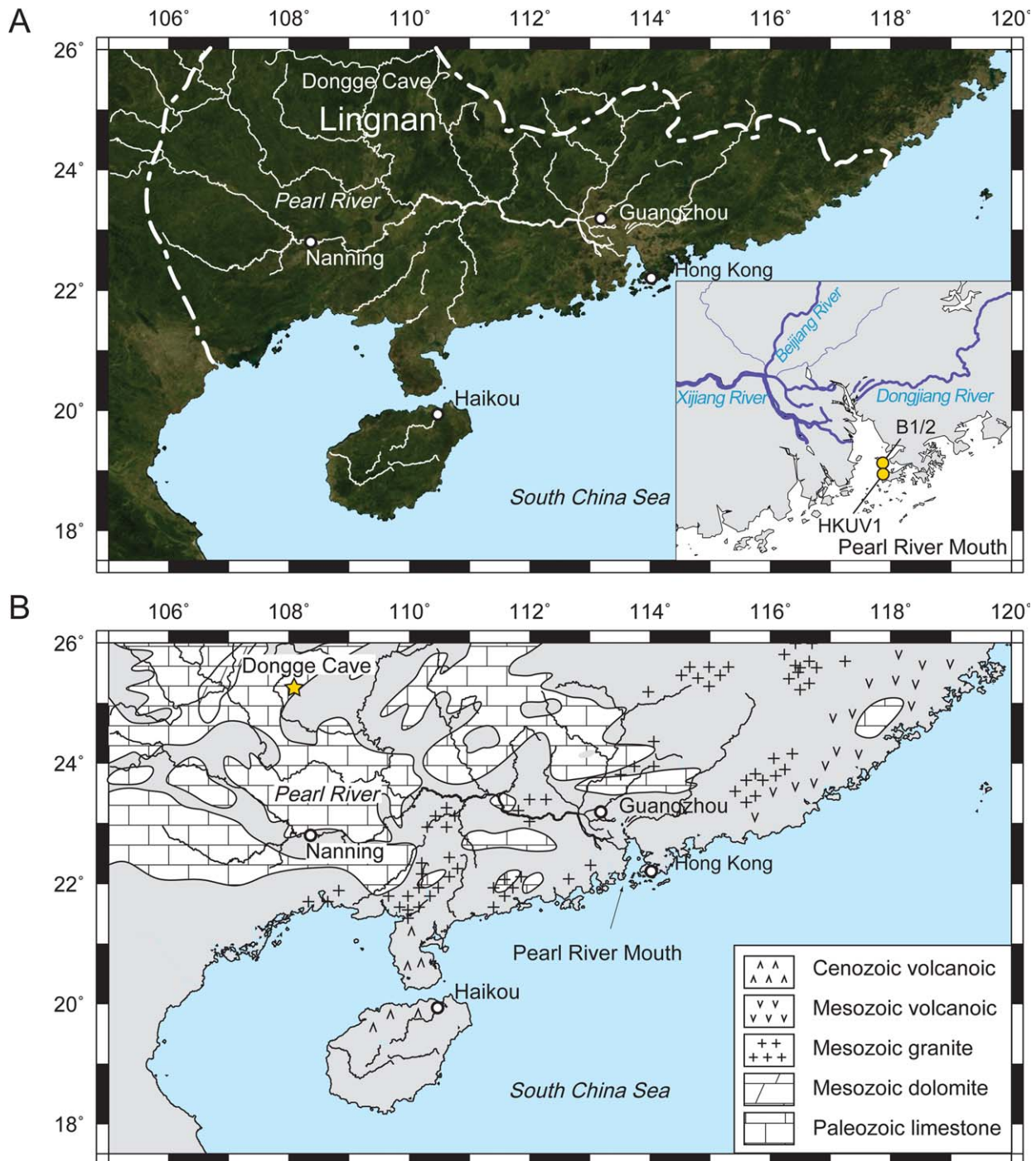
Figure 1.   (a) Satellite image of the Pearl River. Map shows the study sites in the inset map and Dongge Cave, which was the location of speleothem climate studies [*Dykoski et al.*, 2005]. Modern river samples from *Liu et al.* [2007] are shown as white squares. Recent sedimentation at the river mouth is a mixture of sediment from the western (Xijiang), northern (Beijiang) and eastern (Dongjiang) tributaries of the Pearl River. (b) Simplified geological map of the Pearl River basin showing the abundance of carbonate rocks in the western parts of the drainage. Map modified from *Ma et al.* [1998].

the summer. Further inland the central basin is cooler and less humid, with an annual temperature variation of 12–28°C. Most of the precipitation reaching the region falls during the summer, with annual precipitation averaging 150–200 cm/yr close to the delta [*Woo et al.*, 1979]. A variety of

rainfall proxies, most notably the high-resolution speleothem records from Dongge Cave indicate that summer rainfall intensified during the start of the Holocene, ~11 ka [*Dykoski et al.*, 2005], and remained strong until 6–7 ka. Subsequently, the monsoon weakened to a minimum between 2.0 and 3.0 ka.

3. Controls on Sediment Chemistry

[5] Changes to landscape (e.g., physical erosion and chemical weathering) are generally forced by regional climatic conditions, coupled with rock uplift driven by solid Earth tectonic forces. Water-mobile elements such as K are leached from rock by weathering [*Nesbitt and Young*, 1982], increasing the relative proportion of water-immobile elements such as Al or Rb in the resulting sediment. Although many elements are mobilized during chemical alteration the mobile behavior of K is particularly well accepted and together with Na is the most widely analyzed element that behaves in this fashion. Thus, K/Al and K/Rb have been used as weathering proxies in previous studies of sediments deposited on continental margins, including southern China [*Clift et al.*, 2008; *Hu et al.*, 2012]. Other weathering proxies include the $^{87}Sr/^{86}Sr$ of the clay fraction, which increases as chemical weathering of radiogenic silicates strengthens, although this proxy is also affected by provenance and by the proportion of carbonate to silicate weathering [*Derry and France-Lanord*, 1996].

[6] Clay minerals are sensitive to weathering conditions, albeit with response times sometime in excess of 1 myr. [*Singer*, 1984; *Thiry*, 2000]. Kaolinite and smectite are formed by weathering during the chemical breakdown of igneous rocks. The ratios of smectite and kaolinite to physically eroded chlorite and illite have been used as weathering proxies and have been successfully correlated with monsoon variations [*Alizai et al.*, 2012; *Boulay et al.*, 2007; *Chamley*, 1989; *Colin et al.*, 2010; *Wan et al.*, 2006]. Kaolinite is frequently abundant in well-developed soils from regions of tropical climate with high rainfall, whereas warmer, drier conditions with less leaching produce smectite-rich soils [*Hillier*, 1995]. Thus, the ratio of kaolinite/smectite may also be used as an indicator of chemical weathering, especially in identifying tropical conditions that favor kaolinite formation.

[7] Individually, proxies for chemical weathering may be hard to interpret because of the multiple influences over their variation, as discussed below. As a result the most robust weathering reconstructions are ones that are built using a combination of complementary proxies, an approach we follow here.

[8] The composition of sediment reaching the ocean in a major river system reflects the combination of a number of different processes. The bulk composition is clearly largely defined by the source rocks from which the material was initially eroded, although when much of the source rock is carbonate then this material is typically dissolved and that is not represented within the sediments deposited at the river mouth [*Metzger and Harbor*, 1999]. The pristine material removed from the bedrock experiences alteration first during the formation of soils [*Churchman*, 2000] and then further weathering occurs during transport to the ocean. If the sediment is stored en route to the ocean in fluvial terraces then weathering may become significantly advanced even before the sediment reaches the river mouth [*Alizai et al.*, 2012; *Johnsson et al.*, 1991; *Singh et al.*, 2005]. After burial sediment will continue to alter as a result of diagenetic processes, although the Holocene sediments considered in this study are unlikely to have been affected much because of their young age and shallow burial.

[9] Rates of chemical weathering within the floodplain are closely linked to the topography (i.e., tectonics) [*Hren et al.*, 2007], which controls transport processes in the river, as well as the climatic conditions. In general, faster weathering rates are associated with warmer, more humid conditions [*Edmond and Huh*, 1997; *West et al.*, 2005; *White and Blum*, 1995]. The relationship between rainfall and weathering is not however necessarily simple because higher runoff can accelerate transport and provide insufficient time for alteration to advance before the sediment reaches the delta. Furthermore, fast weathering rates do not necessarily result in more weathered sediment if the duration of weathering is insufficient. For example, sediments exposed during relatively dry, cold glacial periods can still be strongly weathered if they have been left exposed for a sufficiently long time [*Limmer et al.*, 2012].

[10] In estuarine settings, sediment composition can be further affected by the sorting of sediment by current activity, either by the river discharge or by tidal influences. Current sorting of mineral grains can also generate geochemical trends that are not driven by variations in weathering. For example, loss of coarse orthoclase but not plagioclase from the sand would result in a reduced K/Al

value for the bulk sediment that is not linked to alteration. Strong current activity may be responsible for erosion and reworking of older deposits, which when mixed with the new discharge can alter the bulk sediment chemistry. Some of this reworking may be linked to variations in sea level because a phase of transgression can result in enhanced reworking close to the advancing shoreline, but would have become less important as sea level stabilized during the Holocene [*Cattaneo and Steel*, 2003]. Thus, we would expect there to be a link between climate change and sediment chemistry and mineralogy provided the bedrocks from which the sediment was derived remained the same, as they do in this study.

4. Materials and Methods

[11] We examined sediment from two cores taken within the Pearl River delta located 4.7 km apart and positioned to the NW of Lantau Island, Hong Kong, directly in the path of Pearl River discharge (Figure 1). Both cores are dominated by muddy sediments with occasional shell-rich intervals, representing high-energy, current-swept periods of sedimentation (Figure 2), although there is very little coarser clastic material. The lack of a coherent change in sediment type makes it unlikely that the geochemistry of the cores would vary in a systematic way as a result of grain size variation. The base of the section studied from Core B2/1 is completely comprised of muds between 12 and 9 mbsf, but over other depth ranges the cores contain regular shell beds. The mud commonly contains large pieces of shell material and in beds up to 15 cm thick we identified shell hash deposits. No evidence is found for sedimentation of coarse quartz sand from neighboring Lantau Island.
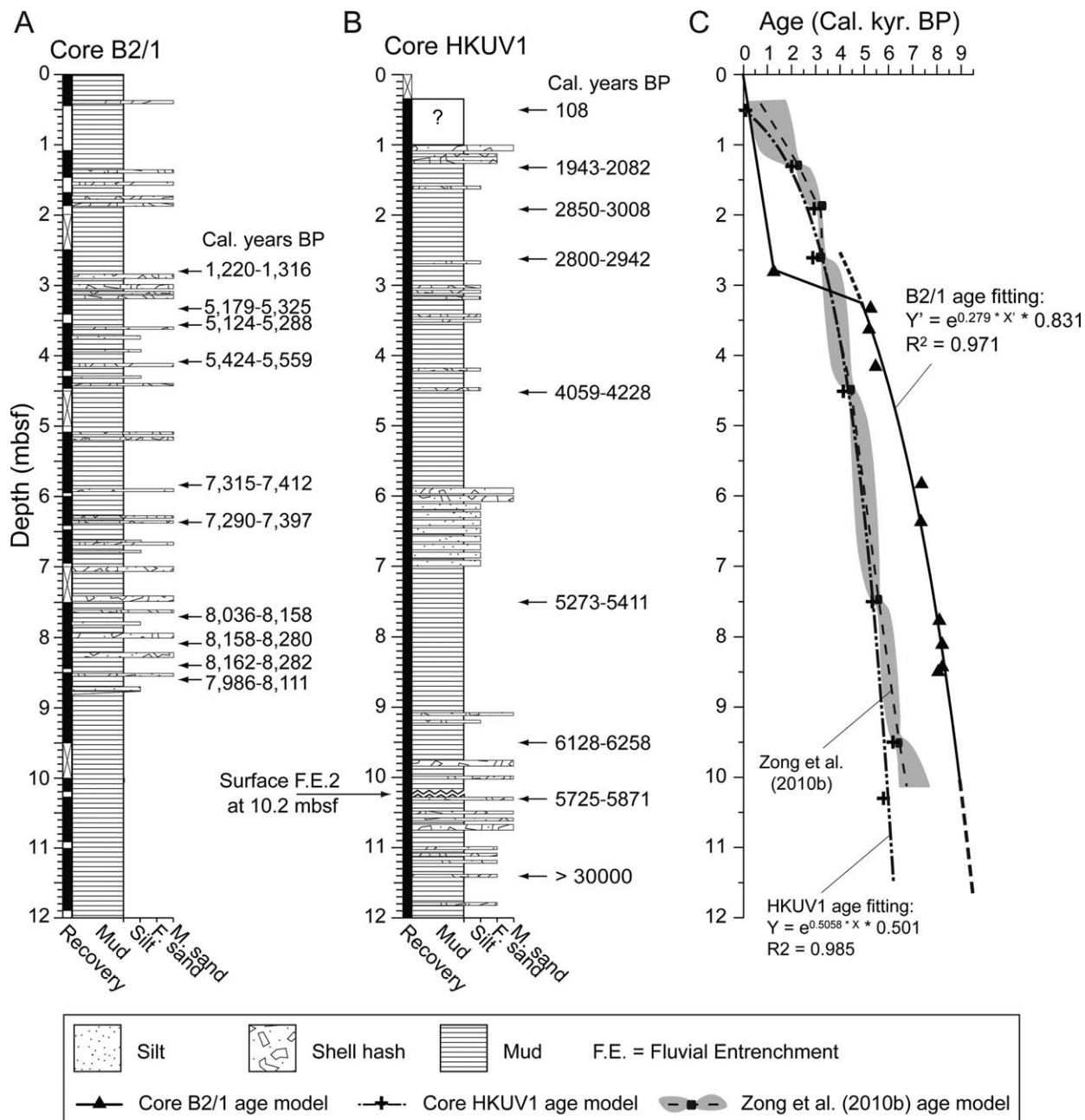
4.1. Age Model

[12] Nine bivalves and one gastropod were selected from the top 12 m of Core B2/1 and were dated by accelerator mass spectrometry (AMS-^{14}C) methods at the Natural Environment Research Council Radiocarbon Facility (Environment), UK. Calibrated ages were calculated using Calib 6.02, applying the marine04 programme [*Stuiver et al.*, 2006] and using a reservoir age correction of -128 ± 40 years for the South China Sea [*Southon et al.*, 2006]. Calibrated results with depth are provided in Table 1. A further nine Holocene ages for

Core HKUV1 were published by *Zong et al.* [2009, 2010a] that we recalibrated using the same reservoir correction. A depth-age for each core was determined by fitting exponential functions to the data (Figure 2). Our model for HKUV1 is almost indistinguishable from that of *Zong et al.* [2010b] (Figure 2c), except that our model is slightly younger toward the base of the section (>10 mbsf). While the age models for HKUV1 and B2/1 deeper than 3 m below seafloor (mbsf) fit to simple curves, we adopt a different model for the top 3 mbsf of Core B2/1 because accumulation rates slowed after ~5.1 ka at that site, but were then very rapid after ~1.2 ka. The shallowest intact bivalve from Core B2/1 from 2.81 mbsf yielded a calibrated age of 1267 years before present (B.P.). This shell was found at the top of a ~30 cm thick muddy layer, including sand-sized carbonate shell hash. An age of 5263 cal years B.P. age was determined from the underlying sediment at a depth of 3.33 mbsf, indicating a period of high-energy erosion or condensed sedimentation at Core B2/1 between these ages. During this period, we use the record from Core HKUV1 to provide the environmental reconstruction. We apply a linear interpolation of ages above 3 mbsf for Core B2/1 in order to convert depths to ages (Figure 2c). By using two cores located close together but with different accumulation rates we are able to build a composite section that adequately covers the past 9.5 ka of sedimentation in the Pearl River delta. Where overlap occurs we note that proxies measured in both cores are generally in close agreement indicating that they are receiving sediment from the same source, as one might expect given their locations.

4.2. Major Elements Analysis

[13] Samples for geochemical analysis were taken every 10 cm in Core HKUV1 and every 8 cm in Core B2/1. Major and trace element analyses were made by conventional X-ray fluorescence (XRF) using a SPECTRO XEPOS benchtop energy dispersive XRF at University of Massachusetts, Boston. Samples were powdered in an agate mill before oxide analysis. Powdered samples (3–5 g dry weight) were measured under a He purge. We used U.S. Geological Survey (USGS) standard Devonian shale-1 as the calibration standard. USGS Green River shale (SGR-1) was analyzed as an unknown to monitor accuracy of the major element analyses. Measured values for SGR-1 were better than 95% of the known values. Reported errors represent the propagated error of repeat/replicate measures and the measured certified (MC) ratio for each element, with uncertainties of <5%.

Figure 2. (a and b) Sedimentary log of the studied section of two cores showing the lithologies, recovery and locations of samples dated by AMS-^{14}C methods. Logs were drawn from direct core description. (c) Our preferred age model uses an exponential fitting. We compare the B2/1 model with the revised age model of Core HKUV1 based on the reported ^{14}C ages from *Zong et al.* [2009, 2010a]. We also show the age model of *Zong et al.* [2010b] for HKUV1 to demonstrate that there is little difference between our preferred model and this earlier model.

Results are provided in Table S1 (supporting information).[1] Carbonate carbon was measured using a UIC coulometer at the Institut für Chemie und

Biologie des Meeres, University of Oldenburg, Germany. This equipment is specifically designed to convert all carbonate (including dolomite) carbon into CO_2. The analysis was performed using half diluted $HClO_4$ at 100°C for at least 7 min in order to ensure complete conversion [*Engleman et*

---

[1]Additional supporting information may be found in the online version of this article.

Table 1. Results of AMS-^{14}C Dating Processed Using the Marine04 Program of Calib 6.02 Program [*Stuiver et al.*, 2006] and a Reservoir Age Correction of -128 ± 40 years [*Southon et al.*, 2006]

Sample ID (Core-Section W/A, Depth Below Section Top)	Depth (mbsf)	Sample Type	$\delta^{13}C$ (‰)	Age Modern (years)	1σ Error (years)	Calibrated Age (years B.P., 1σ)	Median Cal Age (years B.P.)
HKGS_B2/1–3-W, 33 cm	2.81	Bivalve	−1.3	1585	30	1220–1316	1267
HKGS_B2/1–3-W, 83 cm	3.33	Bivalve	0.0	4800	30	5179−5325	5263
HKGS_B2/1–4-W, 13 cm	3.63	Bivalve	1.0	4760	30	5124−5288	5199
HKGS_B2/1–4-W, 66 cm	4.16	Bivalve	−1.6	4975	30	5424−5559	5469
HKGS_B2/1–5-W, 73 cm	5.83	Bivalve	−0.9	6715	30	7315−7412	7361
HKGS_B2/1–6-W, 37 cm	6.37	Bivalve	−0.8	6685	35	7290−7397	7338
HKGS_B2/1–7-A, 27 cm	7.77	Bivalve	−0.5	7515	30	8036−8158	8099
HKGS_B2/1–7-W, 61 cm	8.11	Bivalve	−2.4	7610	30	8158−8280	8213
HKGS_B2/1–7-A, 93 cm	8.43	Gastropod	−0.6	7615	30	8162−8282	8219
HKGS_B2/1–8-W, 0 cm	8.5	Bivalve	−0.6	7460	30	7986−8111	8049

al., 1985]. Uncertainty in accuracy and precision was less than 3% [*Hu et al.*, 2012].

4.3. Isotopic Analysis

[14] Isotope analysis was partly performed at the Open University, UK, using a Neptune Multicollector-Inductively Coupled Plasma-Mass Spectrometer (MC-ICP-MS) for Sr and a Thermo-Finnigan Triton mass spectrometer for Nd. Further samples were analyzed at the Woods Hole Oceanographic Institution (WHOI), USA, using a Neptune MC-ICP-MS for both Sr and Nd. Samples were digested using a standard HF-HNO$_3$ technique. Prior to loading onto the ion exchange columns, samples were centrifuged to remove any residual graphite. Solutions were loaded on to Sr-spec resin in order to separate Sr isotopes, following the procedure outlined by *Deniel and Pin* [2001]. Procedural blanks for these analyses were 20–25 pg for Sr (and 50–70 pg for Nd). The standard NBS 987 was run to monitor machine performance in both laboratories and yielded an average ^{87}Sr/^{86}Sr of 0.710254 ± 19 (27 ppm 2 s.d., $n = 24$), which is within error of the multidynamic thermal infrared multispectral scanner (TIMS) value of ^{87}Sr/^{86}Sr $= 0.710248 \pm 11$ reported by *Thirlwall* [1991].

[15] Nd was extracted by standard column procedures and isotopic compositions were determined on ThermoFinnigan Triton mass spectrometer at the Open University and on an MC-ICP-MS at the WHOI. ^{143}Nd/^{144}Nd values were normalized to ^{146}Nd/^{144}Nd $= 0.7219$ and are quoted relative to 0.511847 for the La Jolla standard from the Open University. For samples analyzed at the WHOI isobaric interferences of ^{87}Rb on ^{87}Sr and ^{86}Kr on ^{86}Sr were corrected for by monitoring ^{82}Kr, ^{83}Kr and ^{85}Rb and by applying a mass bias correction, as described by *Jackson and Hart* [2006]. The La Jolla

standard was measured several times during each analytical session. The internal precision for Nd isotopic measurements is 5–10 ppm (2σ). The external precision, after correction to values for La Jolla standard (0.511847), is approximately 15 ppm (2σ). Nd isotopic values were converted to ε_{Nd} [*DePaolo and Wasserburg*, 1976] that is calculated using a ^{143}Nd/^{144}Nd value of 0.512638 for the chondritic uniform reservoir [*Hamilton et al.*, 1983]. The results of both Sr and Nd analyses are shown in Table 2.

4.4. Clay Mineralogy

[16] Clay mineralogy was determined using a Siemens X-ray diffractometer (XRD) at the James Hutton Institute, Aberdeen, UK, with Co Kα radiation selected by a diffracted beam monochromator. The clay-sized fraction (<2 μm) was prepared for semiquantitative analysis by separating from the rest of sample by application of Stokes' Law through settling. The filter transfer method was used to orient clay minerals on a glass slide prior to XRD analysis following the method of *Moore and Reynolds* [1989]. A set of three diffraction patterns (i.e., air dried, glycolated and heated to 300°C for 1 h) were produced for each sample and used for mineral quantification. Estimates of clay mineral abundances were made by fitting profiles and calculating basal areas of the main clay minerals using Materials Data Inc Jade 6 software on glycolated slides. The fitting approach involves all relevant peaks of clay minerals simultaneously for each attempt and is made continuously with a unique configuration and procedure to reduce systematic error. For clay minerals present in amounts >10 wt% uncertainty is estimated to be better than ± 5 wt% at the 95% confidence level. Uncertainty of peak area measurement based on repeated measurements is typically <5%, with the smallest

Table 2. Sr and Nd Isotope Compositions of Bulk Sediment Measured by MC-ICPMS and TIMS Methods

Sample ID (Core-Section-W/A, Depth Below Section Top)	Depth (mbsf)	Fitted Age (Cal ka)	$^{87}Sr/^{86}Sr$	Standard Error (2σ)	$^{143}Nd/^{144}Nd$	Standard Error (2σ)	ε_{Nd}	TC (%)	TIC (%)
HKUV1-(1.0–2.5 m)-W, 50 cm	1.50	2.17	0.716972	3.7E-06	0.512065	4.7E-06	−11.18	1.12	0.36
HKUV1-(1.0–2.5 m)-W, 100 cm	2.00	2.74	0.717276	3.9E-06	0.512064	3.5E-06	−11.20	1.18	0.31
HKUV1-(2.5–4.0 m)-W, 0 cm	2.50	3.18	0.717126	4.2E-06	0.512110	5.3E-06	−10.29	1.31	0.43[a]
HKUV1-(2.5–4.0 m)-W, 50 cm	3.00	3.54	0.716203	3.5E-06	0.512078	5.2E-06	−10.93	1.26	0.48
HKUV1-(2.5–4.0 m)-W, 100 cm	3.50	3.85	0.717443	4.1E-06	0.512092	5.1E-06	−10.66	1.28	0.32[a]
HKUV1-(4.0–4.8 m)-W, 0 cm	4.00	4.11	0.717605	3.6E-06	0.512075	3.6E-06	−10.97	1.20	0.34
HKUV1-(4.0–4.8 m)-W, 50 cm	4.50	4.35	0.716844	3.0E-06	0.512075	5.8E-06	−10.98	1.31	0.25[a]
HKUV1-(4.8–5.7 m)-W, 20 cm	5.00	4.55	0.718831	3.7E-06	0.512072	3.5E-06	−11.05	1.14	0.28
HKUV1-(4.8–5.7 m)-W, 70 cm	5.50	4.74	0.720495	4.7E-06	0.512086	7.6E-06	−10.76	1.29	0.20[a]
HKUV1-(5.7–6.7 m)-W, 30 cm	6.00	4.92	0.717235	3.9E-06	0.512081	3.6E-06	−10.87	1.11	0.18
HKUV1-(5.7–6.7 m)-W, 80 cm	6.50	5.07	0.718983	7.6E-06	0.512102	1.1E-06	−10.46	1.31	0.19[a]
HKUV1-(6.7–7.6 m)-W, 30 cm	7.00	5.22	0.719669	4.0E-06	0.512076	4.0E-06	−10.97	1.16	0.25
HKUV1-(6.7–7.6 m)-W, 80 cm	7.50	5.36	0.719639	1.5E-06	0.512059	5.1E-06	−11.30	1.30	0.15[a]
HKUV1-(7.6–8.5 m)-W, 40 cm	8.00	5.49	0.718597	3.8E-06	0.512078	6.7E-06	−10.93	1.20	0.27
HKUV1-(8.5–9.5 m)-W, 0 cm	8.50	5.61	0.721521	2.4E-06	0.512158	3.2E-06	−9.36	1.47	0.33[a]
HKUV1-(8.5–9.5 m)-W, 50 cm	9.00	5.72	0.719552	3.6E-06	0.512076	3.2E-06	−10.95	1.20	0.25
HKUV1-(9.5–10.5 m)-W, 0 cm	9.50	5.83	0.718869	6.1E-06	0.512085	4.0E-06	−10.79	1.36	0.00[a]
HKUV1-(9.5–10.5 m)-W, 50 cm	10.00	5.93	0.718035	4.0E-06	0.512076	4.4E-06	−10.97	1.15	0.17
HKGS_B2/1-1-W, 0 cm	0	0	0.723387	6.2E-06	0.512095	1.9E-06	−10.60	0.72	0.11
HKGS_B2/1–2-W, 8 cm	1.08	0.49	0.722824	5.3E-06	0.512128	4.7E-06	−9.95	0.83	0[b]
HKGS_B2/1–2-A, 78 cm	1.78	0.80	0.718505	2.1E-06	0.512068	2.9E-06	−11.12	1.34	0.84
HKGS_B2/1–3-W, 56 cm	3.06	3.19	0.718030	2.9E-06	0.512063	3.8E-06	−11.22	1.23	0.57
HKGS_B2/1–4-W, 24 cm	3.74	5.40	0.720243	3.6E-06	0.512073	2.2E-06	−11.03	0.96	0.26
HKGS_B2/1–4-W, 88 cm	4.38	5.97	0.723108	3.4E-06	0.512050	9.6E-06	−11.47	1.16	0.40
HKGS_B2/1–5-W, 56 cm	5.66	6.89	0.723693	2.7E-06	0.512069	1.3E-06	−11.10	0.97	0[b]
HKGS_B2/1–6-W, 24 cm	6.24	7.24	0.721250	1.8E-06	0.512075	2.1E-06	−10.99	0.94	0.10
HKGS_B2/1–6-W, 88 cm	6.88	7.59	0.722865	5.8E-06	0.512088	4.1E-06	−10.73	0.87	0[b]
HKGS_B2/1–7-W, 48 cm	7.98	8.12	0.720953	2.7E-06	0.512106	2.7E-06	−10.38	0.76	0.16
HKGS_B2/1–8-W, 16 cm	8.66	8.41	0.719259	2.3E-06	0.512127	6.0E-06	−9.97	0.94	0.37
HKGS_B2/1–8-W, 80 cm	9.30	8.67	0.719777	3.1E-06	0.512120	2.1E-06	−10.11	0.73	0.23
HKGS_B2/1–9-W, 40 cm	10.40	9.07	0.719337	3.2E-06	0.512120	3.7E-06	−10.11	0.52	0.13
HKGS_B2/1–10-W, 8 cm	11.08	9.30	0.721567	3.0E-06	0.512108	4.5E-06	−10.35	0.63	0.15
HKGS_B2/1–10-W, 71 cm	11.71	9.49	0.721485	2.7E-06	0.512114	3.6E-06	−10.22	0.55	0.06

[a]Data after *Yang et al.* [2011].
[b]Content less than lower limit of detection.

peaks having the highest uncertainties [*Hillier*, 2003]. Multiple attempts for each slide were made to constrain the randomness of fitting. The results of our analysis are provided in Table 3.

[17] In addition, the proportion of clay-sized particles in the bulk sediment is potentially sensitive to climatic conditions because stronger chemical weathering driven by strong monsoons generates more clay minerals. This proxy has been used to monitor fluvial flux driven by monsoon rainfall in the north South China Sea [*Hu et al.*, 2012; *Wang et al.*, 1999], with heavier monsoon precipitation carrying more fluvial input with higher proportions of clay. However, in shallow water, high-energy conditions such as in the delta setting encountered in this study the effects of current activity may dominate in concentrating clay material in one place, so that this cannot be considered a reliable weathering proxy in this case. Nonetheless, grain size of both cores were measured following the method of *Hu et al.* [2012] to characterize the ma-

terial being analyzed and data are also provided in Table 3.

5. Results

[18] Figure 3 shows how these proxies have varied since 9.5 ka in the Pearl River delta, with depositional age uncertainties shown with error bars on the $^{87}Sr/^{86}Sr$ values derived from the departure of each dated point from the age model curve. ε_{Nd} values were generally constant since 7 ka at around −11 after a fall in values between 8.5 and 7.0 ka. All the weathering proxies vary in a coherent fashion suggestive of a gradual linked evolution rather than random scatter. The fine-grained character of the muds analyzed is consistent with a prodelta sedimentary setting (Figure 2), and with the coherent geochemical evolution that does not involve local influences. Between 9.5 and 6.0 ka K/Al and K/Rb decreased slightly, while clay proportion and $^{87}Sr/^{86}Sr$ increased. Each proxy then

Table 3. Results of Clay Mineral Analysis of Samples Taken From Core HKUV1 and Core B2/1[a]

Sample ID (Core-Section W/A, Depth Below Section Top)	Depth (mbsf)	Fitted Age (Cal ka)	Smectite (%)	Illite (%)	Kaolinite (%)	Chlorite (%)	Clay (%)
HKUV1-(1.0–2.5 m)-W, 0 cm	1.00	1.37	9	55	34	2	37
HKUV1-(1.0–2.5 m)-W, 10 cm	1.10	1.56	20	46	23	11	47
HKUV1-(1.0–2.5 m)-W, 20 cm	1.20	1.73	29	43	15	13	33
HKUV1-(1.0–2.5 m)-W, 30 cm	1.30	1.89	19	45	21	15	31
HKUV1-(1.0–2.5 m)-W, 40 cm	1.40	2.03	33	42	21	4	27
HKUV1-(1.0–2.5 m)-W, 50 cm	1.50	2.17	30	44	13	13	27
HKUV1-(1.0–2.5 m)-W, 60 cm	1.60	2.30	28	50	11	11	29
HKUV1-(1.0–2.5 m)-W, 70 cm	1.70	2.42	33	45	14	7	29
HKUV1-(1.0–2.5 m)-W, 80 cm	1.80	2.53	28	48	16	8	30
HKUV1-(1.0–2.5 m)-W, 90 cm	1.90	2.64	41	43	13	3	30
HKUV1-(1.0–2.5 m)-W, 100 cm	2.00	2.74	43	42	7	8	29
HKUV1-(1.0–2.5 m)-W, 110 cm	2.10	2.84	42	41	12	4	29
HKUV1-(1.0–2.5 m)-W, 120 cm	2.20	2.93	40	42	8	10	29
HKUV1-(1.0–2.5 m)-W, 130 cm	2.30	3.02	33	46	19	3	31
HKUV1-(1.0–2.5 m)-W, 140 cm	2.40	3.10	38	43	9	11	29
HKUV1-(2.5–4.0 m)-W, 0 cm	2.50	3.18	34	44	14	8	26
HKUV1-(2.5–4.0 m)-W, 10 cm	2.60	3.26	35	46	8	10	31
HKUV1-(2.5–4.0 m)-W, 20 cm	2.70	3.33	36	43	11	10	30
HKUV1-(2.5–4.0 m)-W, 30 cm	2.80	3.41	38	43	16	3	32
HKUV1-(2.5–4.0 m)-W, 40 cm	2.90	3.48	44	38	7	11	31
HKUV1-(2.5–4.0 m)-W, 50 cm	3.00	3.54	42	38	17	3	29
HKUV1-(2.5–4.0 m)-W, 60 cm	3.10	3.61	37	40	15	7	30
HKUV1-(2.5–4.0 m)-W, 70 cm	3.20	3.67	34	45	8	12	33
HKUV1-(2.5–4.0 m)-W, 80 cm	3.30	3.73	37	43	13	7	31
HKUV1-(2.5–4.0 m)-W, 90 cm	3.40	3.79	34	42	11	12	34
HKUV1-(2.5–4.0 m)-W, 100 cm	3.50	3.85	40	39	10	12	33
HKUV1-(2.5–4.0 m)-W, 110 cm	3.60	3.90	37	42	9	12	34
HKUV1-(2.5–4.0 m)-W, 120 cm	3.70	3.96	34	41	13	13	34
HKUV1-(2.5–4.0 m)-W, 130 cm	3.80	4.01	33	41	14	12	31
HKUV1-(2.5–4.0 m)-W, 140 cm	3.90	4.06	37	43	8	12	35
HKUV1-(4.0–4.8 m)-W, 0 cm	4.00	4.11	29	45	10	16	27
HKUV1-(4.0–4.8 m)-W, 10 cm	4.10	4.16	34	39	23	3	37
HKUV1-(4.0–4.8 m)-W, 20 cm	4.20	4.21	36	39	15	10	36
HKUV1-(4.0–4.8 m)-W, 30 cm	4.30	4.26	35	41	18	7	34
HKUV1-(4.0–4.8 m)-W, 40 cm	4.40	4.30	33	41	22	4	35
HKUV1-(4.0–4.8 m)-W, 50 cm	4.50	4.35	37	38	17	8	36
HKUV1-(4.0–4.8 m)-W, 60 cm	4.60	4.39	35	40	11	14	36
HKUV1-(4.0–4.8 m)-W, 70 cm	4.70	4.43	37	37	13	13	37
HKUV1-(4.8–5.7 m)-W, 0 cm	4.80	4.47	31	40	23	6	27
HKUV1-(4.8–5.7 m)-W, 10 cm	4.90	4.51	34	39	15	11	30
HKUV1-(4.8–5.7 m)-W, 20 cm	5.00	4.55	32	41	14	13	38
HKUV1-(4.8–5.7 m)-W, 30 cm	5.10	4.59	31	40	17	12	37
HKUV1-(4.8–5.7 m)-W, 40 cm	5.20	4.63	33	37	14	15	35
HKUV1-(4.8–5.7 m)-W, 50 cm	5.30	4.67	32	41	15	13	33
HKUV1-(4.8–5.7 m)-W, 60 cm	5.40	4.71	29	41	20	10	33
HKUV1-(4.8–5.7 m)-W, 70 cm	5.50	4.74	31	37	18	14	32
HKUV1-(4.8–5.7 m)-W, 80 cm	5.60	4.78	32	40	14	15	37
HKUV1-(5.7–6.7 m)-W, 0 cm	5.70	4.81	34	39	23	4	36
HKUV1-(5.7–6.7 m)-W, 10 cm	5.80	4.85	31	43	16	10	34
HKUV1-(5.7–6.7 m)-W, 20 cm	5.90	4.88	33	44	21	3	36
HKUV1-(5.7–6.7 m)-W, 30 cm	6.00	4.92	30	41	16	12	38
HKUV1-(5.7–6.7 m)-W, 50 cm	6.20	4.98	30	40	20	11	37
HKUV1-(5.7–6.7 m)-W, 60 cm	6.30	5.01	30	40	16	14	40
HKUV1-(5.7–6.7 m)-W, 70 cm	6.40	5.04	28	45	15	12	40
HKUV1-(5.7–6.7 m)-W, 80 cm	6.50	5.07	35	38	23	4	39
HKUV1-(5.7–6.7 m)-W, 90 cm	6.60	5.10	30	40	26	3	39
HKUV1-(6.7–7.6 m)-W, 0 cm	6.70	5.13	31	42	18	9	36
HKUV1-(6.7–7.6 m)-W, 10 cm	6.80	5.16	33	41	21	5	37
HKUV1-(6.7–7.6 m)-W, 20 cm	6.90	5.19	30	41	13	16	36
HKUV1-(6.7–7.6 m)-W, 30 cm	7.00	5.22	37	36	15	12	37
HKUV1-(6.7–7.6 m)-W, 40 cm	7.10	5.25	30	39	13	18	41
HKUV1-(6.7–7.6 m)-W, 50 cm	7.20	5.28	30	39	29	2	39
HKUV1-(6.7–7.6 m)-W, 60 cm	7.30	5.30	29	42	13	16	40
HKUV1-(6.7–7.6 m)-W, 70 cm	7.40	5.33	32	41	12	14	42
HKUV1-(6.7–7.6 m)-W, 80 cm	7.50	5.36	30	41	14	14	38
HKUV1-(7.6–8.5 m)-W, 0 cm	7.60	5.38	34	38	20	8	38

Table 3. (continued)

Sample ID (Core-Section W/A, Depth Below Section Top)	Depth (mbsf)	Fitted Age (Cal ka)	Smectite (%)	Illite (%)	Kaolinite (%)	Chlorite (%)	Clay (%)
HKUV1-(7.6–8.5 m)-W, 10 cm	7.70	5.41	31	37	19	13	39
HKUV1-(7.6–8.5 m)-W, 20 cm	7.80	5.44	34	36	21	8	38
HKUV1-(7.6–8.5 m)-W, 30 cm	7.90	5.46	35	35	14	16	41
HKUV1-(7.6–8.5 m)-W, 40 cm	8.00	5.49	36	38	14	12	43
HKUV1-(7.6–8.5 m)-W, 50 cm	8.10	5.51	35	36	25	4	29
HKUV1-(7.6–8.5 m)-W, 60 cm	8.20	5.53	29	40	24	7	35
HKUV1-(7.6–8.5 m)-W, 70 cm	8.30	5.56	30	38	14	18	40
HKUV1-(7.6–8.5 m)-W, 80 cm	8.40	5.58	36	35	14	16	35
HKUV1-(8.5–9.5 m)-W, 0 cm	8.50	5.61	29	40	14	17	34
HKUV1-(8.5–9.5 m)-W, 10 cm	8.60	5.63	32	38	13	17	31
HKUV1-(8.5–9.5 m)-W, 20 cm	8.70	5.65	31	41	12	16	32
HKUV1-(8.5–9.5 m)-W, 30 cm	8.80	5.67	35	36	13	16	32
HKUV1-(8.5–9.5 m)-W, 40 cm	8.90	5.70	32	39	20	9	32
HKUV1-(8.5–9.5 m)-W, 50 cm	9.00	5.72	31	40	27	2	32
HKUV1-(8.5–9.5 m)-W, 60 cm	9.10	5.74	33	38	15	15	31
HKUV1-(8.5–9.5 m)-W, 70 cm	9.20	5.76	32	37	28	3	33
HKUV1-(8.5–9.5 m)-W, 80 cm	9.30	5.78	30	39	15	16	33
HKUV1-(8.5–9.5 m)-W, 90 cm	9.40	5.80	31	39	15	15	34
HKUV1-(9.5–10.5 m)-W, 0 cm	9.50	5.83	30	38	25	6	37
HKUV1-(9.5–10.5 m)-W, 10 cm	9.60	5.85	33	37	19	11	34
HKUV1-(9.5–10.5 m)-W, 20 cm	9.70	5.87	32	38	16	15	36
HKUV1-(9.5–10.5 m)-W, 30 cm	9.80	5.89	35	35	27	2	36
HKUV1-(9.5–10.5 m)-W, 40 cm	9.90	5.91	30	41	12	17	36
HKUV1-(9.5–10.5 m)-W, 50 cm	10.00	5.93	34	36	19	11	39
HKUV1-(9.5–10.5 m)-W, 60 cm	10.10	5.95	32	38	29	1	45
HKUV1-(9.5–10.5 m)-W, 70 cm	10.20	5.97	33	36	30	2	47
HKGS_B2/1-1-W, 0 cm	0.00	0.00	9	46	43	2	32
HKGS_B2/1-1-W, 24 cm	0.24	0.11	8	44	45	3	46
HKGS_B2/1-1-W, 40 cm	0.40	0.18	12	46	38	4	44
HKGS_B2/1–2-W, 8 cm	1.08	0.49	6	44	46	4	39
HKGS_B2/1–2-W, 32 cm	1.32	0.60	23	43	31	3	30
HKGS_B2/1–2-A, 57 cm	1.57	0.71	20	43	37	0	28
HKGS_B2/1–2-A, 78 cm	1.78	0.80	29	47	20	4	27
HKGS_B2/1–3-W, 8 cm	2.58	1.16	17	47	33	2	35
HKGS_B2/1–3-W, 24 cm	2.74	1.24	26	43	26	5	23
HKGS_B2/1–3-W, 40 cm	2.90	1.96	37	42	20	1	25
HKGS_B2/1–3-W, 56 cm	3.06	3.19	30	44	23	4	30

[a]Proportion of clay-sized particles (<4 μm) in the bulk sediment also provided following method of *Hu et al.* [2012].

shows a much clearer reverse trend from that time to ~2.5 ka. K/Al data from Core B2/1 also show falling values from 6 ka until ~2.5 ka, but the data points are not very numerous because this is a period of slow sedimentation at this site. After ~2.5 ka K/Al, K/Rb and smectite/(illite + chlorite), decreased and clay proportion, kaolinite/illite, kaolinite/smectite (not plotted) and $^{87}Sr/^{86}Sr$ increased sharply to the present day. Although smectite/(illite + chlorite) values are slightly higher in Core B2/1 than they are in HKUV-1 between 2.5 ka and the present they appear to be within error and show the same general trend given the variability, and uncertainty in the age control for both cores.

[19] We note that the period 1.3–5.2 ka is condensed in Core B2/1 so that the transition from less weathered into more weathered sediment starting around 2.5 ka is only well recorded in Core HKUV1. The transitions to different range of values of both clay mineral content ratios plotted

appear to be mismatched between two core sites, but given the age uncertainties and the condensed character of the sanction we do not consider this difference to be significant. We emphasize that the absence of a preserved record in Core B2/1 only represents a preservation issue and does not argue that the trends seen in Core HKUV1 are not robust or applicable to the whole river mouth. Indeed, before and after this hiatus period the cores show remarkable agreement in the value of the various proxies, suggesting that making a composite section from the two cores is justifiable and provides the best opportunity for an expanded high-resolution records covering the entire 9.5 ka of the study.

6. Discussion

6.1. Weathering and the Monsoon

[20] The proxies described above can be interpreted to indicate a modest increase in chemical
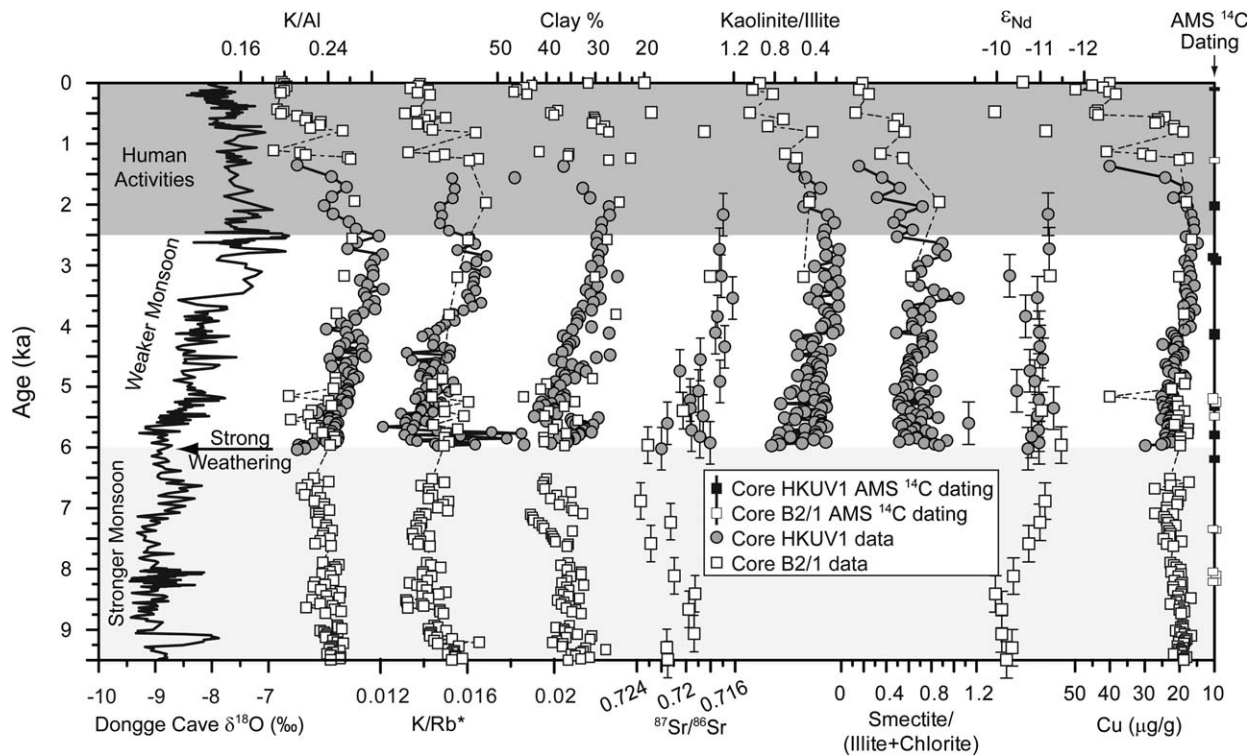
Figure 3. Weathering and anthropogenic proxies. These show stronger chemical weathering prior to 6000 years ago, which is a time of strong summer rainfall and after ∼2000 years ago when monsoonal climate had only strengthened slightly after a minimum between 3.5 and 2.0 ka based on the Dongge speleothem [*Dykoski et al.*, 2005]. The change since 2.0 ka correlates with increasing Cu abundances (data by this study combined with reported data by *Zong et al.* [2010a]). Age uncertainties are shown as error bars on Sr and Nd isotope results, but are the same for the other proxy data too. Depositional age uncertainties are equivalent to the departure of each dated point from the age model curve.

weathering intensity from 9.5 to 6.0 ka, followed by a sharper decrease until 3 ka. Chemical weathering was very weak between 3.5 and 2.5 ka, as shown by the high values of K/Al, K/Rb and smectite/(illite + chlorite), as well as low values of kaolinite/illite and $^{87}Sr/^{86}Sr$ (Figure 3). After 2.5 ka there was a sharp increase toward the present day, indicating that the sediment reaching the delta has become more altered. The rise in K/Al and K/Rb may partly reflect the preferential sorting of minerals by current activity because we see that they rise as the proportion of clay falls. However, the progressive addition of orthoclase grains in sand, which might drive the observed changes in K/Al and K/Rb would not affect $^{87}Sr/^{86}Sr$ values, yet our analyses demonstrate that Sr isotopes are also evolving over the same time period in a coherent fashion. Likewise, the changing smectite/(illite + chlorite), kaolinite/illite, and kaolinite/smectite (not plotted) values are not greatly affected by current sorting of minerals because the hydrodynamic

properties of different clays are not so great as to cause the trends that we observe.

[21] We recognize that current sorting of clay minerals has been noted in modern delta settings resulting in changing ratios moving offshore [*Lykousis et al.*, 1981], and while differential settling and flocculation have been shown to be insignificant, estuarine circulation can be important in controlling ratios where there are different mineral suites available [*Feuillet and Fleischner*, 1980]. However, in the case of the cores considered here neither of these influences is likely to be significant, because the core sites have been proximal to the river mouth for most of the Holocene and other sources of clay beyond the Pearl River are not available. Indeed, the results of *Lykousis et al.* [1981] showed that smectite is favored in the river mouth and declines offshore, while our reconstruction shows the reverse trend since 3 ka despite a modest progradation of the river mouth toward the sites. As a result we argue that changes in clay

Geochemistry
Geophysics
Geosystems

G^3

HU ET AL.: WEATHERING IN HOLOCENE SOUTHERN CHINA

10.1002/ggge.20166

mineral assemblage reflect a reduction in chemical alteration prior to 3.0 ka and followed by an increase between 2.5 ka and the present. This indicates that the trends in K/Al and K/Rb are at least partly driven by weathering intensity.

[22] The potential control of climate over this weathering process can be determined by comparison with a suitable reconstruction and we here employ the speleothem rainfall record from Dongge Cave [*Dykoski et al.*, 2005], which lies in the northern Pearl River basin (Figure 1). Our records show a close correlation between changes in weathering intensity of the sediment deposited at the delta and monsoon strength. The weakening of weathering intensity between 7.0 and 3.0 ka corresponds well to the decreasing summer rainfall through this period. The correlation is however less good after 2.5 ka when many weathering proxies sharply increased back to values seen earlier in the Holocene, but at a time when the monsoon only strengthened very slightly. For example, δ^{18}O values in the recent past are equivalent to those seen around 3.5 ka, but do not reach the high values observed at 7–9 ka, even though the degree of alteration in the delta sediments as tracked by K/Al values is now at the same intensity as sediment deposited at that earlier time. We conclude that variations in monsoon intensity are likely the primary control on the intensity of weathering in Pearl River delta sediment during the Early-Mid Holocene.

[23] One reason for this may be that a drier climate linked to monsoon weakening from 7.0 to 3.5 ka caused alteration rates to decrease so that less weathered sediment reached the delta during that period. Such a model requires an almost instantaneous change in weathering intensity following the change in climate, an interpretation that has been questioned [*Thiry*, 2000]. Clearly, it takes time for changing reaction rates to cause a change in weathering states and in this case the duration would have to be close to the uncertainties in the age model, generally no more than a few hundred years. Alternatively, and more likely, the deposition of strongly weathered material may reflect the influence of older sediment that is being reworked into the river as a result of processes such as channel incision in flood plains. Stronger incision during periods of wet summer monsoon could result in the flux to the delta becoming more weathered. *Giosan et al.* [2012] recently demonstrated just such an incision in the monsoonal Indus River flood plains during the Early Holocene and although the ages of terraces in the Pearl River

have not been defined there is documentation that suitable terraces do exist within this system [*Yuan and Liang*, 1990]. In this case the more weathered material deposited during the Early Holocene would not represent an immediate response to a wetter climate, but rather a reworking of sediment that was weathered at some unknown time in the geological past.

6.2. Provenance Effects

[24] Our interpretation of linked weathering and monsoon intensity is consistent with most geological studies over longer time periods [*Derry and France-Lanord*, 1996], provided that provenance variations can be excluded because these can also affect the measured proxies. In this study, we use Nd isotopes to track evolving provenance because these have a long history of being effective in resolving sources [*Draut et al.*, 2002; *Liu et al.*, 2007] and are known to be largely unaffected by chemical weathering processes [*Goldstein and Jacobsen*, 1988]. Although some of the bulk sediment signal may be related to autogenetic coatings this is only a factor when considering the coatings on Nd-poor particles such as foraminifera, whereas clastic sediment is dominated by the composition of the grain itself [*Bayon et al.*, 2002; *Rutberg et al.*, 2000]. We note a close correspondence between ε_{Nd} values in our sediments and that both in the river [*Liu et al.*, 2007], as well as in the bedrock (Figure 4), consistent with the bulk sediment signal being driven by provenance not a marine overprint. The change in ε_{Nd} values between 8.5 and 7.0 ka suggests a shift in the source of sediment to slightly older, more continental sources at that time. This could be achieved either by changes in the location of erosion driven by changing climate or by drainage reorganization. As a result the increase in ^{87}Sr/^{86}Sr values between 8.5 and 7.0 ka partly reflects changing source. However, the dramatic increase in K/Al and decrease in clay mineralogical proxies and ^{87}Sr/^{86}Sr from 6.0 to 3.0 ka, followed by a reverse trend since 2.5 ka are not associated with coherent changes in ε_{Nd} values, and are thus interpreted to mostly reflect changes in weathering intensity. The general lack of correlation between the weathering proxies and ε_{Nd} values, especially after 7 ka when monsoon rainfall weakened, indicates that provenance and mineral sorting by current activity are not a significant controls over weathering intensity in this study.

[25] The decrease in ε_{Nd} values from −10 to −11 between 8.5 and 7 ka could be related to the
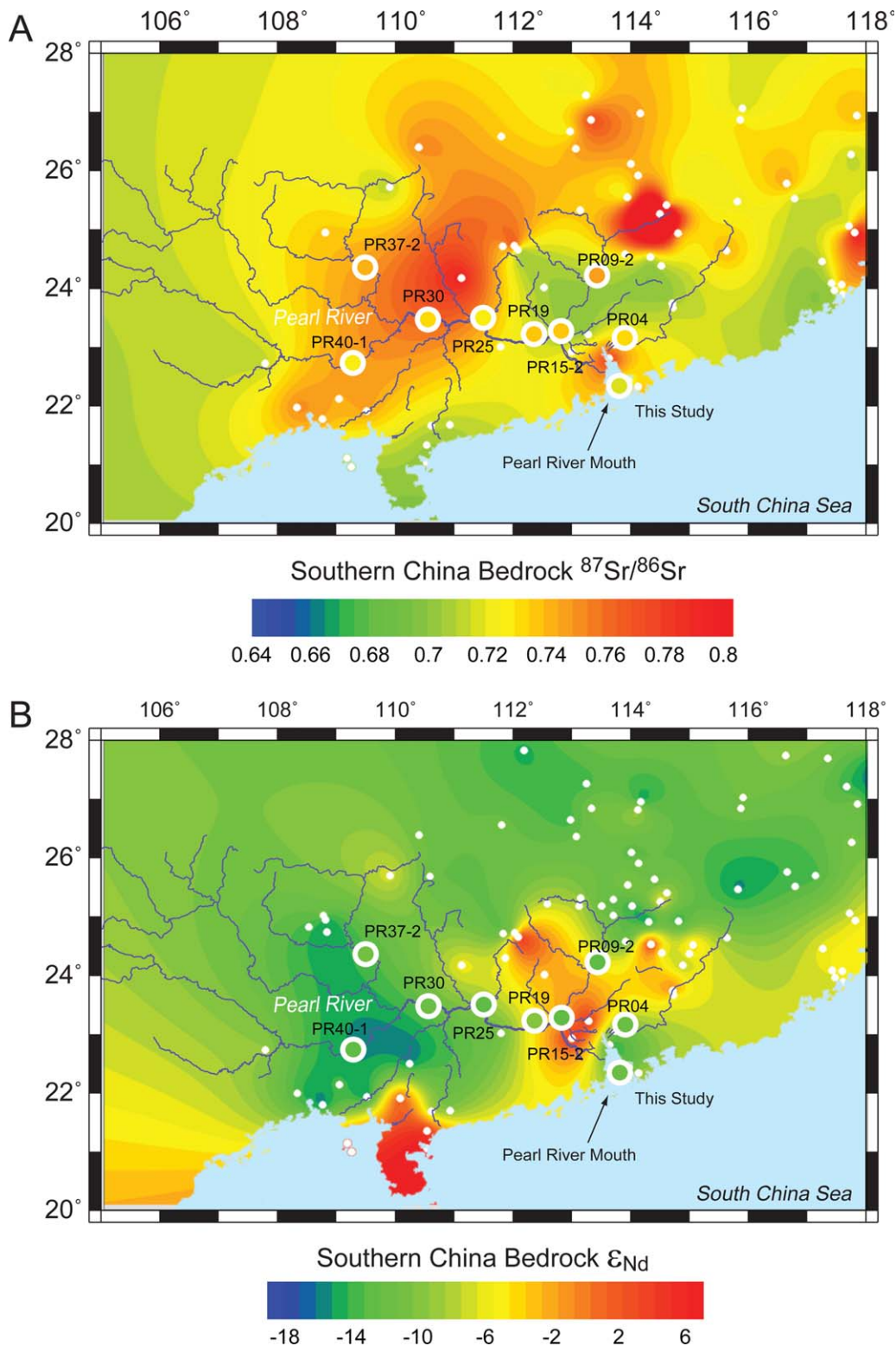
Figure 4.   (a) Contoured map of $^{87}Sr/^{86}Sr$ values of bedrocks exposed in southern China derived from published data of Creta-ceous, mostly igneous rocks collected by *Chen and Jahn* [1998], *Darbyshire et al.* [1997] as well as results from the GEOROC compilation (http://georoc.mpch-mainz.gwdg.de/). These show no direct comparison between the bedrock and modern river sediments [*Liu et al.*, 2007] shown as circle symbols. (b) ε_{Nd} values for bedrocks exposed in southern China compiled from the same sources as for Sr. This map shows that the bedrocks north of the delta have higher ε_{Nd} values compared to much of the river basin.

progressive progradation of the Pearl River delta during the Holocene, and possibly to the changing influence of the eastern and northern tributaries compared to the main Xijiang (western) branch. It is possible, albeit unlikely, that some of the geochemical and mineralogical changes reconstructed could reflect the varying supply from sources supplied from the different tributaries that differ in these proxies but not in ε_{Nd} values. However, we note that *Liu et al.* [2007] show little difference between the eastern and western parts of the modern Pearl River basin in terms of either clay mineralogy or isotope composition. We argue that changing influence from eastern and western tributaries is unlikely to drive the observed trends because reconstructions of the delta show mixing between these tributaries much further north than the core sites, even early in the Holocene with no possibility of direct sediment supply only from the eastern Dongjiang to the core sites [*Zong et al.*, 2009].

[26] We further examined the degree of known isotopic heterogeneity in the regional bedrock in order to see whether changes in sediment source could have been an influence in the past despite the evidence from modern river sediments that suggests this should not be important. $^{87}Sr/^{86}Sr$ and ε_{Nd} values for the bedrocks were compiled from *Chen and Jahn* [1998], *Darbyshire and Sewell* [1997] and GEOROC (http://georoc.mpch-mainz.gwdg.de) and were gridded using a simple Kriging method with a linear variogram model (Slope = 1, Aniso = 1, 0). The results are shown a contoured map in Figure 4. We also show the character of modern river sediment [*Liu et al.*, 2007] shown as circles colored using the same scale as the bedrock data.

[27] Modern river sediment $^{87}Sr/^{86}Sr$ and ε_{Nd} values vary within the range of the measured bedrocks in the drainage basin, but do not correlate directly with the local bedrock values at the sample point because the river is integrating sediment from the entire upstream area at each sample point. Integration is the reason we see less variation in isotopic ratios in modern river sediments compared to the bedrock. In any case, the modern river is also eroding weathered soils that are altered compared to the bedrocks plotted in the data compilation. Although it is clear that $^{87}Sr/^{86}Sr$ values are lower in the area north of the delta (~24°N, 113°E) these sources influence all tributaries and are not specific to east or west. The eastern Dongjiang River tribtuary seems to have

fewer sources with very high $^{87}Sr/^{86}Sr$ values (red colors on Figure 4) compared to the other two tributaries, but this is not reflected by high $^{87}Sr/^{86}Sr$ values in the modern river sediment, presumably because of nonuniform erosion of the bedrock. We also note that bedrock data density is low in the western parts of the basin and it is unclear whether a coherent difference really exists at a large scale across the basin, or if this is an artifact of incomplete coverage. For example, the high $^{87}Sr/^{86}Sr$ value in the central Xijiang basin (~111°E) is the result of a single sample location.

[28] We further note that bedrocks to the north of the delta are more positive in ε_{Nd} compared to those exposed further the west. However, the modern river sediments do not show much difference between the two regions, suggesting that bedrock sampling by earlier studies may not be representative of the average bedrock composition, or that sediment production is not even across each river basin. Moreover, the modern river sediment does not change composition significantly passing through the region of high ε_{Nd} values, indicating that these rocks contribute only a modest part of the total sediment load.

[29] We conclude that the modern river sediments do not show large coherent differences between the different parts of the basin. We therefore infer that drainage capture or delta reorganization and growth were not the cause of the geochemical variations seen during the 9.5 ka history presented in this paper.

6.3. Carbonate Influence on $^{87}Sr/^{86}Sr$ Variation

[30] Direct comparison of the sediment in the cores presented here and those from the modern river [*Liu et al.*, 2007] is not possible in terms of $^{87}Sr/^{86}Sr$ because the river samples were analyzed after removal of carbonate material, while our samples were analyzed in bulk. This raises the possibility that the variation we see in $^{87}Sr/^{86}Sr$ values is controlled by carbonate contents not by weathering. Our cores were taken from the mouth of the Pearl River and contain low concentrations of carbonate (mostly <0.4%), except for the presence of relatively large bivalve shells that were removed in sampling. In addition, carbonate is eroded from the extensive limestone source regions of southern China into the sediment. Although it is impossible to know exactly what impact this carbonate makes on the $^{87}Sr/^{86}Sr$
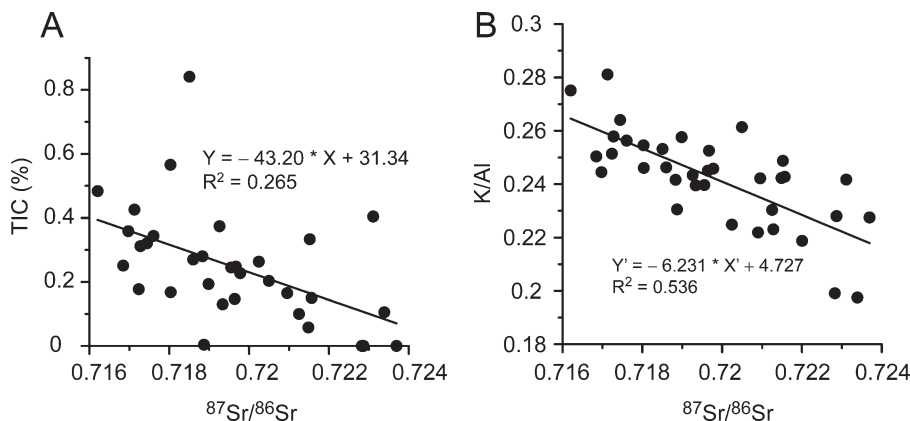
Figure 5. (a) $^{87}Sr/^{86}Sr$ variations show a modest correlation with TIC components in the sediment, (b) while there is a better correlation with K/Al ratios suggesting a stronger role for chemical weathering in controlling $^{87}Sr/^{86}Sr$.

composition we can make estimates about what might reasonably be expected and thus quite how much weathering information can be derived from the $^{87}Sr/^{86}Sr$ values.

[31] Our measurement of total inorganic carbon (TIC) accounts for both the detrital carbonate eroded from southern China as well as any shell fragments. The presence of this carbonate will tend to reduce $^{87}Sr/^{86}Sr$ values and indeed our samples are consistently lower than those reported from decarbonated samples from the modern river [*Liu et al.*, 2007]. However, our analyses show that the TIC contents are low, almost all <0.4% and largely <0.2%, suggesting that this influence may be modest. Considering that an average silicate sediment from the Pearl River contains ~100 ppm Sr [*Liu et al.*, 2007] and a detrital carbonate has 1000 ppm Sr, then the addition of 0.4% TIC would cause the bulk $^{87}Sr/^{86}Sr$ value to fall from 0.7240 to 0.7199. The observed change in TIC from 0–0.1% at 7 ka to ~0.4% at 3 ka should therefore cause $^{87}Sr/^{86}Sr$ to fall from 0.724 to around 0.7199. However, the $^{87}Sr/^{86}Sr$ values actually falls to 0.717, indicating that TIC variations are not the only control on $^{87}Sr/^{86}Sr$ values of the bulk sediment and may account for around half of the total variability.

[32] We further investigate the reduction of $^{87}Sr/^{86}Sr$ values caused by the presence of carbonate fractions that outcrop in the western part of the river basin by comparing to the values measured from bulk sediments in the Pearl River delta. This shows that the carbonate in the Pearl River delta sediment has only caused limited change to the bulk sediment $^{87}Sr/^{86}Sr$. We provide further information of this in the supporting information.

[33] We identify a rough negative correlation between $^{87}Sr/^{86}Sr$ and TIC concentrations that argues for some TIC control on $^{87}Sr/^{86}Sr$ values, as we calculated above (Figure 5a). However, we also note that $^{87}Sr/^{86}Sr$ values vary much more closely with K/Al and clay mineral assemblage, neither of which are controlled by carbonate contents. In Figure 5b, we show that $^{87}Sr/^{86}Sr$ values correlate better with K/Al compared to TIC. We conclude that although $^{87}Sr/^{86}Sr$ is partly controlled by detrital carbonate contents the effect of weathering on this ratio is also important in this study. If $^{87}Sr/^{86}Sr$ is used with other carbonate-independent weathering proxies then it can play a part in reconstructing the changing weathering intensity of sediment in our cores but is not useful by itself.

[34] It is interesting to note that between 7.0 and 3.5 ka TIC increases at the same time as K/Al, even though these proxies need not have any linkage. This suggests that they are both being controlled by a dominant process, likely climatic conditions. We can envisage that a changing monsoon may increase the relative erosional flux of carbonate bedrocks in the western Pearl River basin, as the erosion patterns migrate, and at the same time reduce reworking of older weathered materials from fluvial terraces. Thus, the falling $^{87}Sr/^{86}Sr$ values for this time would reflect both source and weathering influences, driven by a single climatic control.

[35] Although the presence of carbonate introduces uncertainty in the interpretation of $^{87}Sr/^{86}Sr$ values we suggest that these are more controlled by weathering intensity than by carbonate content. By itself $^{87}Sr/^{86}Sr$ is not a robust weathering proxy
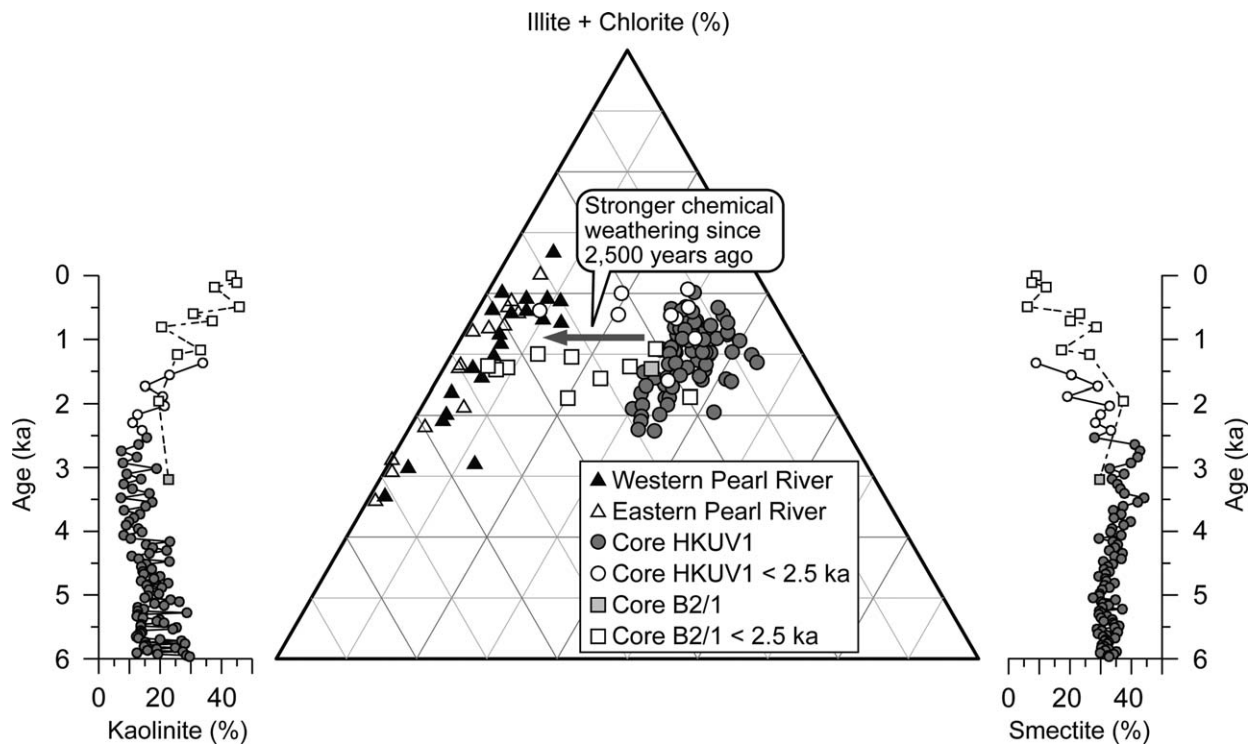
Figure 6. Differences between modern and Holocene river. Plot shows the striking difference in clay mineralogy between Holocene delta sediment and the modern river as measured by *Liu et al.* [2007]. Sediment younger than ∼2500 years shows a shift toward the smectite-poor, kaolinite-rich compositions of the modern river.

but its coherency with those proxies that are not affected by the presence of carbonate means that it is consistent with the trends of changing weathering in southern China through the Holocene.

6.4. Anthropogenic Influences

[36] The trend to stronger weathering since 2.5 ka can be further understood by reference to the composition of modern river sediments. Figure 6 shows that modern river sediments have consistently higher kaolinite and less smectite compared to the Holocene delta sediments [*Liu et al.*, 2007]. This demonstrates that the modern river is now in a disturbed state compared to much of the Holocene and explains why there is so little smectite in the modern river but so much in the cores. We note that the higher modern kaolinite contents are a continuation of an increasing trend observed since 2.5 ka. Kaolinite is the product of intense tropical weathering. Why should the modern river carry so much strongly weathered sediment when the change in monsoon climate has been so modest since 2.5 ka? We suggest that the change in river sediment has been caused by widespread human settlement of the Pearl River basin. While climate

change cannot explain the abundance of strongly weathered material, the large-scale disturbance of older, weathered soils by the onset of widespread and intensive agriculture would be an effective mechanism to rework older weathered materials into the river system [*Milliman et al.*, 2008; *Syvitski et al.*, 2005]. Using the abundance of Cu and Pb (not shown) in the sediment as a proxy for human activities we see a close correlation between the timing of human settlement and the change in river sediment composition (Figure 3). *Lv and Liu* [2011] have measured Cu concentrations in the modern river at Guangzhou to vary from 120 to 425 ppm, far above even the highest levels in our cores, confirming that this metal is a pollutant introduced by human activity.

[37] Increased ploughing as agriculture spread would be expected to drive up sediment delivery to the delta. However, mass accumulation rates reduce at the top of Core HKUV1, although they have been very fast at B2/1 since 1.3 ka. These discrepancies highlight why regional sediment budgets cannot be made from single cores in a diverse and heterogeneous setting like a delta but require at least 2-D seismic data to define sediment volumes.

Use of two cores to look at changing mass fluxes is not a reliable proxy for erosion across the basin.

[38] Changes in $\delta^{13}C$ also occur after 2 ka, indicating a shift in the average flora of the basin. The increase in $\delta^{13}C$ values is driven by a change in favor of C4 plants compared to C3. *Zong et al.* [2010a] interpreted that this largely reflects the onset of sugar cane agriculture in the river basin. The natural plants in this area today are dominantly C3 plants, mixed with some C4 grasses, including C4 sugarcane, which is one of the major agricultural products in the lower deltaic area [*Yu et al.*, 2010]. Taken together we see a dramatic change in river chemistry initiating at the same time that other proxies show widespread human settlement, but when climate is relatively stable. There remains little systematic archeobotanical evidence relating to early agriculture in the Pearl River delta, adjacent parts of Guangdong or the greater Pearl River catchment. This is because archeological research in this region has been disproportionately focused on excavation of burials and typological study of artifacts, ceramics, and bronzes, recovered from such contexts [e.g., *Higham*, 1996; *Wei*, 2008; *Zhao*, 2007]. Nevertheless, what archaeological evidence is available provides a general outline of when cultivation first began, when settlement and presumably agricultural populations increased, and during which periods these processes intensified.

[39] Throughout the Middle and Early Holocene, in the Pearl River delta, like elsewhere in the Lingnan region (southernmost China), human populations were hunter-gatherer-fishers, including interior groups who exploited freshwater resources, often associated with evidence from cave sites, and coastally focused groups who exploited marine resources. Migration into the hills of northern Guangdong occurred after 6 ka [*Fuller*, 2011; *Zhang and Hung*, 2012; *Zhao*, 2011], with the first agriculture, based on rice, being introduced between 5.0 and 4.0 ka, although finds remain few and focused on the southern mountain slopes and north of the Pearl River delta [*Fuller et al.*, 2010; *Zhang and Hung*, 2010]. In eastern Guangdong agricultural settlement is thought to start from 4.2 ka [*Wei*, 2008], although the sparse archaeological evidence implies low population densities.

[40] It is only from the Bronze Age (~3.5 ka) that increased evidence from burials and settlements suggests the beginnings of sedentism, i.e., permanent agricultural villages, implying more prolonged land use, rather than groups focused on wild resources,

including aquatic resources. This period, equivalent to the Shang through Zhou eras of central China (~3.5–2.4 ka) provides increasing evidence for settlement along the whole of the Pearl River system, especially from the Western Zhou, from ~3.0 ka onward [*Higham*, 1996]. This period saw increasing cultural unity across Guangdong prior to the conquest of the Pearl River Delta by the Qin Dynasty, before 2.2 ka [*Wei*, 2008]. This unity increased societal interaction and population densities.

[41] In the Pearl River delta written sources indicating population increase of more than eight fold over the period between ~2.0 and 1.0 ka [*Marks*, 2006]. While it is unclear when sugarcane cultivation became established in the region, it was certainly a major crop by the Song Dynasty (~1.0 ka) [*Bray and Needham*, 1984]. The overall picture is a process of increasing agricultural production and supporting population. The first major shift toward more intensive agriculture may date back to ~2.5 ka, identified as the transition of a "natural" to "cultural" geography by *Zhao* [2007], while subsequent intensification took place in the Han period (2.2–1.8 ka) and increasingly thereafter.

7. Conclusions

[42] Our study demonstrates that the degree of alteration of sediments deposited in the Pearl River delta since 9.5 ka has undergone coherent variations that closely parallel reconstructed summer monsoon strength in southern China, at least until 2.5 ka. After 6.0 ka changes in chemical weathering are not linked to changing sources or drainage reorganization but follow a pattern tracking monsoon intensity. One possibility is that strong summer rains cause stronger weathering in the flood plains that is then communicated rapidly to the delta. If so then the lag in response is too short to be measured with the ^{14}C age control available in this study. Alternatively and more likely, the deposition of strongly weathered sediment reflects enhanced reworking of older fluvial sediment stored in terraces and eroded during times of heavier monsoon rain. In its natural state then the composition of Pearl River sediment is strongly controlled by environmental conditions, but reworking is not always a natural process. After 2.5 ka there is only modest increase in monsoon strength at a time, when sediment alteration in the delta is very high. We ascribe this decoupling to enhanced reworking of older weathered soils into the river as a result of spreading

agriculture across the region. The modern river is highly disturbed relative to its compositional state as recently 2.5 ka. The modern river is thus a poor proxy for understanding the typical erosional flux from southern China to the South China Sea, e.g., the modern river is poor in smectite despite being rich in smectite through much of the Holocene.

[43] The onset of the landscape disturbance comes somewhat after the initial human settlement of the area, because small-scale agriculture is known to have started by the late Neolithic, around 4.5 ka [*Zhang and Hung*, 2010]. However, the population density was low and focused on coastal fishing, with limited cultivation largely on the hills north of the delta region [*Zhao*, 2007]. Increasing trade, bronze production, and cemetery evidence suggests the sedentary agricultural population began to increase from the late Bronze Age after ~2.7 ka, with further agricultural expansion including wet rice farming, and mulberry and silk worm production from ~2.2 ka [*Lo*, 1996]. At this time it is estimated that half a million people were settled in the Pearl River basin, which equates to a population density of only one person per square kilometer [*Marks*, 2006]. Thus, we suggest that the environmental impact observed in our cores closely followed the widespread settlement of the region and its incorporation into the Chinese empire. The acceleration of weathering between 2.5 and 1.5 ka correlates with a major influx of settlers following warfare and disturbance in northern China [*Marks*, 2006]. We conclude that human activities have had an impact on erosion and landscape in southern China since 2.5 ka that is equivalent to that experienced as a result of monsoon intensification after the onset of the Holocene.

Acknowledgments

References

Alizai, A., S. Hillier, P. D. Clift, and L. Giosan (2012), Clay mineral variations in Holocene terrestrial sediments from the Indus Basin: A response to SW Asian monsoon variability, *Quat. Res.*, *77*(3), 368–381, doi:10.1016/j.yqres.2012.01.008.

Bayon, G., C. R. German, R. M. Boella, J. A. Milton, R. N. Taylor, and R. W. Nesbitt (2002), An improved method for extracting marine sediments fractions and its application to Sr and Nd isotopic analysis, *Chem. Geol.*, *187*, 179–199.

Boulay, S., C. Colin, A. Trentesaux, S. Clain, Z. Liu, and C. Lauer-Leredde (2007), Sedimentary responses to the Pleistocene climatic variations recorded in the South China Sea, *Quat. Res.*, *68*(1), 162–172.

Bray, F., and J. Needham (1984), *Science and Civilisation in China: Volume 6, Biology and Biological Technology, Part 2, Agriculture*, Cambridge Univ. Press, Cambridge, U. K.

Cattaneo, A., and R. J. Steel (2003), Transgressive deposits: A review of their variability, *Earth Sci. Rev.*, *62*, 187–228.

Chamley, H. (1989), *Clay Mineralogy*, 623 pp., Springer, Berlin, Germany.

Chen, D., M. E. Tucker, M. Jiang, and J. Zhu (2001), Long-distance correlation between tectonic-controlled, isolated carbonate platforms by cyclostratigraphy and sequence stratigraphy in the Devonian of South China, *Sedimentology*, *48*(1), 57–78.

Chen, J., and B.-M. Jahn (1998), Crustal evolution of southeastern China: Nd and Sr isotopic evidence, *Tectonophysics*, *284*, 101–133.

Churchman, G. J. (2000), *The Alteration and Formation of Soil Minerals by Weathering*, 459 pp., CRC Press, Boca Raton, Fla.

Clift, P., N. Shimizu, G. Layne, J. Blusztajn, C. Gaedicke, H. Schluter, M. Clark, and S. Amjad (2001), Development of the Indus Fan and its significance for the erosional history of the Western Himalaya and Karakoram, *Bull. Geol. Soc. Am.*, *113*(8), 1039–1051.

Clift, P. D., K. Hodges, D. Heslop, R. Hannigan, L. V. Hoang, and G. Calves (2008), Greater Himalayan exhumation triggered by early Miocene monsoon intensification, *Nature Geosci.*, *1*, 875–880, doi:10.1038/ngeo351.

Colin, C., G. Siani, M.-A. Sicre, and Z. Liu (2010), Impact of the East Asian monsoon rainfall changes on the erosion of the Mekong River basin over the past 25,000 yr, *Mar. Geol.*, *271*(1-2), 84–92, doi:10.1016/j.margeo.2010.01.013.

Darbyshire, D. P. F., and R. J. Sewell (1997), Nd and Sr isotope geochemistry of plutonic rocks from Hong Kong: Implications for granite petrogenesis, regional structure and crustal evolution, *Chem. Geol.*, 143, 81–93.

Deniel, C., and C. Pin (2001), Single-stage method for the simultaneous isolation of lead and strontium from silicate samples for isotopic measurements, *Anal. Chimi. Acta*, *426*(1), 95–103.

DePaolo, D. J., and G. J. Wasserburg (1976), Inferences about magma sources and mantle structure from variations of $^{143}Nd/^{144}Nd$, *Geophys. Res. Lett.*, *3*(12), 743–746.

Derry, L. A., and C. France-Lanord (1996), Neogene Himalayan weathering history and river $^{87}Sr/^{86}Sr$; impact on the marine Sr record, *Earth Planet. Sci. Lett.*, *142*, 59–74.

Draut, A., P. Clift, R. Hannigan, G. Layne, and N. Shimizu (2002), A model for continental crust genesis by arc accretion: Rare earth element evidence from the Irish Caledonides, *Earth Planet. Sci. Lett.*, *203*(3-4), 861–877.

Dykoski, C. A., R. L. Edwards, H. Cheng, D. Yuan, Y. Cai, M. Zhang, Y. Lin, J. Qing, Z. An, and J. Revenaugh (2005), A high-resolution, absolute-dated Holocene and deglacial Asian monsoon record from Dongge Cave, China, *Earth Planet. Sci. Lett.*, *233*(1-2), 71–86.

Edmond, J. M., and Y. Huh (1997), Chemical weathering yields from basement and orogenic terrains in hot and cold climates, in *Tectonic Climate and Climate Change*, edited by W. F. Ruddiman, pp. 330–353, Plenum, New York, N. Y.

Engleman, E. E., L. L. Jackson, and D. R. Norton (1985), Determination of carbonate carbon in geological materials by coulometric titration, *Chem. Geol.*, 53, 125–128.

Feuillet, J. P., and P. Fleischner (1980), Estuarine circulation: Controlling factor of clay-mineral distribution in James river estuary, Virginia, *J. Sediment. Petrol.*, 50, 267–279.

Fuller, D. (2011), Pathways to Asian civilizations: Tracing the origins and spread of rice and rice cultures, *Rice*, 4(3), 78–92, doi:10.1007/s12284-011-9078-7.

Fuller, D., Y.-I. Sato, C. Castillo, L. Qin, A. Weisskopf, E. Kingwell-Banham, J. Song, S.-M. Ahn, and J. van Etten (2010), Consilience of genetics and archaeobotany in the entangled history of rice, *Archaeol. Anthropol. Sci.*, 2(2), 115–131, doi:10.1007/s12520-010-0035-y.

Garrels, R. M., and F. T. MacKenzie (1971), *Evolution of Sedimentary Rocks*, 397 pp., Norton, New York, N. Y.

Giosan, L., P. D. Clift, M. G. Macklin, D. Q. Fuller, S. Constantinescu, J. A. Durcan, T. Stevens, G. A. Duller, A. R. Tabrez, and K. Gangal (2012), Fluvial landscapes of the Harappan civilization, *Proceedings of the National Academy of Sciences*, 109(26), E1688-E1694.

Goldstein, S. J., and S. B. Jacobsen (1988), Nd and Sr isotopic systematics of river water suspended material; Implications for crustal evolution, *Earth Planet. Sci. Lett.*, 87(3), 249–265.

Hamilton, P. J., R. K. Onions, D. Bridgwater, and A. Nutman (1983), Sm-Nd Studies of Archean metasediments and metavolcanics from West Greenland and their implications for the earths early history, *Earth Planet. Sci. Lett.*, 62(2), 263–272.

Higham, C. (1996), *The Bronze Age of Southeast Asia*, 381 pp. Cambridge Univ. Press, Cambridge, U. K.

Hillier, S. (1995), Erosion, sedimentation, and sedimentary origin of clays, in *Clays and the Environment*, edited by B. Velde, pp. 162–219, Springer, Berlin.

Hillier, S. (2003), Quantitative analysis of clay and other minerals in sandstones by X-ray powder diffraction (XRPD), in *Clay Mineral Cements in Sandstones*, edited by R. H. Worden and S. Morad, pp. 213–251, Int. Assoc. Sedimentol, New York, N. Y.

Hren, M. T., G. E. Hilley, and C. P. Chamberlain (2007), The relationship between tectonic uplift and chemical weathering rates in the Washington Cascades: Field measurements and model predictions, *Am. J. Sci.*, 307, 1041–1063, doi:10.2475/09.2007.01.

Hu, D., P. Böning, C. M. Köhler, S. Hillier, N. Pressling, S. Wan, H. J. Brumsack, and P. D. Clift (2012), Deep sea records of the continental weathering and erosion response to East Asian monsoon intensification since 14 ka in the South China Sea, *Chem. Geol.*, 326–327, 1–18, doi:10.1016/j.chemgeo.2012.07.024.

Jackson, M. G., and S. R. Hart (2006), Strontium isotopes in melt inclusions from Samoan basalts: Implications for heterogeneity in the Samoan plume, *Earth and Planetary Science Letters*, 245(1–2), 260–277, doi:10.1016/j.epsl.2006.02.040.

Jahn, B. M., X. H. Zhou, and J. L. Li (1990), Formation and tectonic evolution of Southeastern China and Taiwan: Isotopic and geochemical constraints, *Tectonophysics*, 183, 145–160.

Johnsson, M. J., R. F. Stallard, and N. Lundberg (1991), Controls on the composition of fluvial sands from a tropical weathering environment: Sands of the Orinoco River drainage basin, Venezuela and Colombia, *Geol. Soc. Am. Bull.*, 103(12), 1622–1647, doi:10.1130/0016-7606(1991)103.

Limmer, D. R., P. Boening, L. Giosan, C. Ponton, C. M. Köhler, M. J. Cooper, A. R. Tabrez, and P. D. Clift (2012), Geochemical record of holocene to recent sedimentation on the western Indus continental shelf, Arabian Sea, *Geochem. Geophys. Geosyst.*, 13, Q01008, doi:10.1029/2011GC0038 45.

Liu, Z., C. Colin, W. Huang, K. P. Le , S. Tong, Z. Chen, and A. Trentesaux (2007), Climatic and tectonic controls on weathering in south China and Indochina Peninsula: Clay mineralogical and geochemical investigations from the Pearl, Red, and Mekong drainage basins, *Geochem. Geophys. Geosyst.*, 8, Q05005, doi:10.1029/2006GC001490.

Lo, C. P. (1996), Environmental impact on the development of agricultural technology in China: The case of the dike-pond ('jitang') system of integrated agriculture-aquaculture in the Zhujiang Delta of China, *Agric. Ecosyst. Environ.*, 60(2–3), 183–195, doi:10.1016/s0167–8809(96)01068-7.

Lv, W., and G. Liu (2011), The bioavailability of the heavy metals in the surface sediment from Pearl River Guangzhou section, paper presented at 2011 International Conference on Electrical and Control Engineering (ICECE), Guangzhou, China, 16–18 Sep, IEEE.

Lykousis, V., M. B. Collins, and G. Ferentinos (1981), Modern sedimentation in the N. W. Aegean Sea, *Mar. Geol.*, 43, 111–130.

Ma, L., X. Ding, and B. Fan (1998), *Geological Map of China, Geol*. Publ. House, Beijing.

Marks, R. (2006), *Tigers, Rice, Silk, and Silt: Environment and Economy in Late Imperial South China*, 383 pp., Cambridge Univ. Press, Cambridge, U. K.

Metzger, C., and D. Harbor (1999), Dissolution of carbonate rocks in the upper James River basin; how much sediment is delivered to the coastal plain?, *Va. J. Sci.*, 50(2), 1–148.

Milliman, J. D., K. L. Farnsworth, P. D. Jones, K. H. Xu, and L. C. Smith (2008), Climatic and anthropogenic factors affecting river discharge to the global ocean, 1951–2000, Global Planet. *Change*, 62, 187–194.

Moore, D., and R. Reynolds (1989), *X-Ray Diffraction and the Identification and Analysis of Clay Minerals*, 332 pp., Oxford Univ. Press, Oxford, U. K.

Nesbitt, H. W., and G. M. Young (1982), Early Proterozoic climates and plate motions inferred from major element chemistry of lutites, *Nature*, 299(5885), 715–717.

Ru, K., and J. D. Pigott (1986), Episodic rifting and subsidence in the South China Sea, *AAPG Bull.*, 70(9), 1136–1155.

Rutberg, R. L., S. R. Hemming, and S. L. Goldstein (2000), Reduced North Atlantic deep water flux to the glacial southern ocean inferred from neodymium isotope ratios, *Nature*, 405, 935–938, doi:10.1038/35016049.

Shao, J., S. Yang, and C. Li (2012), Chemical indices (CIA and WIP) as proxies for integrated chemical weathering in China: Inferences from analysis of fluvial sediments, *Sediment. Geol.*, 265–266, 110–120, doi:10.1016/j.sedgeo.2012.03.020.

Singer, A. (1984), The Paleoclimatic interpretation of clay minerals in sediments—A review, *Earth Sci. Rev.*, 21, 251–293.

Singh, M., M. Sharma, and H. J. Tobschall (2005), Weathering of the Ganga alluvial plain, northern India: Implications

from fluvial geochemistry of the Gomati River, *Appl. Geochem.*, 20, 1–21.

Southon, J., M. Kashgarian, M. Fontugne, B. Metivier, and W. W. S. Yim (2006), Marine reservoir corrections for the Indian Ocean and Southeast Asia, *Radiocarbon*, 44(1), 167–180.

Stuiver, M., P. J. Reimer, and T. F. Braziunas (2006), High-precision radiocarbon age calibration for terrestrial and marine samples, *Radiocarbon*, 40, 1127–1151.

Syvitski, J. P. M., V. C., A. J. Kettner, and P. Green (2005), Impact of humans on the flux of terrestrial sediment to the global coastal ocean, *Science*, 308, 376–380.

Thirlwall, M. F. (1991), Long-term reproducibility of multi-collector Sr and Nd isotope ratio analysis, *Chem. Geol.*, 94(2), 85–104.

Thiry, M. (2000), Palaeoclimatic interpretation of clay minerals in marine deposits; An outlook from the continental origin, *Earth Sci. Rev.*, 49(1-4), 201–221.

Wan, S., A. Li, P. Clift, and H. Jiang (2006), Development of the East Asian summer monsoon: Evidence from the sediment record in the South China Sea since 8.5 Ma, *Palaeogeogr. Palaeoclimatol. Palaeoecol.*, 241(1), 139–159.

Wan, S., W. M. Kürschner, P. D. Clift, A. Li, and T. Li (2009), Extreme weathering/erosion during the Miocene climatic optimum: Evidence from sediment record in the South China Sea, *Geophys. Res. Lett.*, 36, L19706, doi:10.1029/2009GL040279.

Wang, L., M. Sarnthein, H. Erlenkeuser, J. Grimalt, P. Grootes, S. Heilig, E. Ivanova, M. Kienast, C. Pelejero, and U. Pflaumann (1999), East Asian monsoon climate during the Late Pleistocene: High-resolution sediment records from the South China Sea, *Mar. Geol.*, 156(1), 243–282.

Wang, Y. J., H. Cheng, R. L. Edwards, Z. S. An, J. Y. Wu, C.-C. Shen, and J. A. Dorale (2001), A high-resolution absolute-dated late Pleistocene monsoon record from Hulu Cave, China, Science, 294, 2345–2348.

Wei, J. (2008), Archaeology culture of East Guangdong region and work in coordination with the environment, Relics South, 1, 019.

West, A. J., A. Galy, and M. J. Bickle (2005), Tectonic and climatic controls on silicate weathering, *Earth Planet. Sci. Lett.*, 235, 211–228, doi:10.1016/j.epsl.2005.03.020.

White, A. F., and A. E. Blum (1995), Effects of climate on chemical weathering in watersheds, *Geochim. Cosmochim. Acta*, 59(9), 1729–1747.

Woo, M.-k., L. Huang, S. Zhang, and Y. Li (1979), Rainfall in Guangdong province, South China, *Catena*, 29, 115–129.

Yang, S., M. Tang, W. W. S. Yim, Y. Zong, G. Huang, A. D. Switzer, and Y. Saito (2011), Burial of organic carbon in Holocene sediments of the Zhujiang (Pearl River) and Changjiang (Yangtze River) estuaries, *Mar. Chem.*, 123(1-4), 1–10, doi:10.1016/j.marchem.2010.07.001.

Yu, F., Y. Zong, J. M. Lloyd, G. Huang, M. J. Leng, C. Kendrick, A. L. Lamb, and W. W.-S. Yim (2010), Bulk organic δ13C and C/N as indicators for sediment sources in the Pearl River delta and estuary, southern China, *Estuarine Coastal Shelf Sci.*, 87(4), 618–630, doi:10.1016/j.ecss.2010.02.018.

Yuan, J., and Z. Liang (1990), Geologic features and ages of second-order river terraces in the Zhujiang River delta, *Acta Sci. Nat. Univ. Sunyatseni*, 4, 102–106.

Zhang, C., and H.-C. Hung (2010), The emergence of agriculture in southern China, *Antiquity*, 84(323), 11–25.

Zhang, C., and H.-C. Hung (2012), Later hunter-gatherers in southern China, 18,000–3000 BC, *Antiquity*, 86(331), 11–29.

Zhao, S. (2007), Environmental change and cultural evolution of pre-qin times in the Pearl River delta, *Huaxia Archaeol.*, 2, 90–97.

Zhao, Z. (2011), New archaeobotanic data for the study of the origins of agriculture in China, *Curr. Anthropol.*, 52(S4), S295–S306.

Zong, Y., G. Huang, A. Switzer, F. Yu, and W. W. S. Yim (2009), An evolutionary model for the Holocene formation of the Pearl River delta, China, *Holocene*, 19(1), 129–142.

Zong, Y., F. Yu, G. Huang, J. Lloyd, and W. Yim (2010a), Sedimentary evidence of late Holocene human activity in the Pearl River delta, China, *Earth Surf. Process. Landforms*, 35, 1095–1102.

Zong, Y., F. Yu, G. Huang, J. M. Lloyd, and W. W. S. Yim (2010b), The history of water salinity in the Pearl River estuary, China, during the late quaternary, *Earth Surf. Process. Landforms*, 35(10), 1221–1233, doi:10.1002/esp.2030.